Journal of Membrane Science and Research 4 (2018) 74-84

Journal of Membrane Science & Research

journal homepage: www.msrjournal.com

Research Paper

Nanoparticles Retention Potential of Multichannel Hollow Fiber Drinking Water Production Membrane

Morgane Le Hir [1], Yvan Wyart [1], Gaëlle Georges [2], Laure Siozade [2], Philippe Moulin [1,*]

[1] *Aix Marseille Université, CNRS, Centrale Marseille, M2P2 UMR 7340, Equipe Procédés Membranaires (EPM), Europôle de l'Arbois, BP80, Pavillon Laennec, Hall C, 13545 Aix en Provence Cedex, France*
[2] *Aix Marseille Université, CNRS, Centrale Marseille, Institut FRESNEL, UMR 7249, 13013, Marseille, France*

Article info

Received 2017-07-30
Revised 2017-10-11
Accepted 2017-10-12
Available online 2017-10-12

Keywords

Ultrafiltration
Fluorescent nanoparticles
Membrane fouling
Characterization
CLSM

Highlights

- Retention potential of nanoparticles by hollow fiber UF membrane
- Distribution profile of membrane fouling by fluorescent nanoparticles
- Membrane characterization by combining multi-scale technics

Graphical abstract

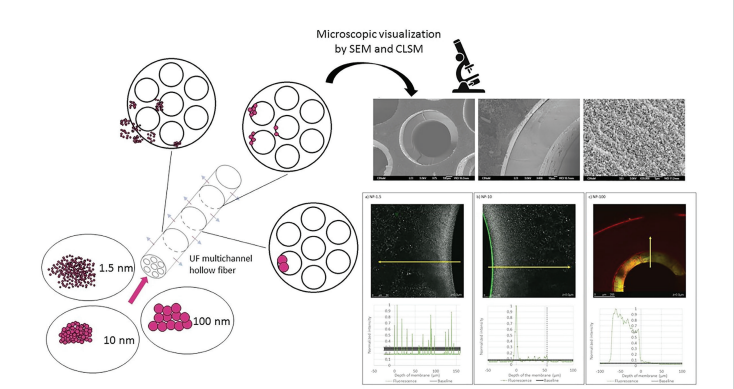

Abstract

This study aims to investigate the potential of nanoparticle retention of ultrafiltration (UF) multichannel hollow fiber membrane. Filtration experiments of fluorescent silica nanoparticles (NPs) (10 and 100 nm) and CdTe quantum dots (1.5 nm) suspensions were carried out under different operating conditions to analyze the retention rate (RT), the fouling zone and the membrane productivity. Fouling mechanism occurring during the experiment has been correlated with the distribution profiles of NPs obtained during the membrane autopsy after filtration by Confocal Laser Scanning Microscopy (CLSM). Results show that large NPs are totally retained on the membrane surface. Medium NPs pass through the membrane at the beginning of the filtration and are gradually stopped in the membrane skin before forming a deposit on the membrane surface. The retention rate of small NPs also increases over time and an in-depth fouling of the membrane (skin + support) has been identified. Mass balance and determination of NPs surface deposit thickness, in the case of a filtration cake, determined by CLSM and scanning electron microscopy (SEM) allowed the estimation of NPs amount trapped in the membrane structure (skin or support) and have been compared to the fouling resistance observed during the filtration run. The CLSM analysis of the membrane on its section presents, in that study, a significant interest because of the high accuracy of the measures: 538.16 nm compared to the 5000 nm reported in a previous study.

1. Introduction

Since the 1980s, the place that nanotechnology occupies has increased and offered opportunities in many sectors due to new properties acquired at the nanoscale [1]. However, the applications involving engineered nanoparticles (NPs) can lead to a release into the environment and to the inevitable discharge, in water, of new and various nanometric-sized materials, the properties of which are still unclear [2–6]. It is difficult to clearly define the NPs removal potential offered by a drinking water plant. Previous studies [7] have reported that the coagulation, flocculation, sedimentation and sand filtration would remove about 20%-90% and 60%-97% of NPs, respectively. The ozonation step, even if it was not initially thought to be a NPs removal

* Corresponding author at: Phone: +33 4 42 90 85 01; fax: +33 4 42 90 85 15
E-mail address: philippe.moulin@univ-amu.fr (Ph. Moulin)

DOI: 10.22079/JMSR.2017.69079.1150

step, would affect the aqueous matrix and would facilitate NPs removal. During the activated carbon filtration, carbon and NPs charge and ionic strength can lead to the removal of NPs [7].

For 30 years, membrane filtration has been used alone or integrated in drinking water production line and allowed to obtain clarified and disinfected water. Previous studies have shown that membrane filtrations could be used to distinguish by fractionation large particulate (>18 µm), particulate (2–18 µm), colloidal/nanoparticle (10 kDa–0.2 µm) and truly dissolved fractions (<10 kDa) in river water samples [8]. Membrane filtration therefore presents a great potential for NPs retention [7, 9–11]. It is important to clearly understand the behaviour of these NPs during the filtration, the objective being to retain a maximum of NPs on the membrane surface to limit in depth fouling of the membrane, in order to limit process productivity decrease and to facilitate membranes backwash. In fact, Decaloris et al. [12] showed that the pre-treatment by ferric chloride which increases the particle floc size can lead to a decrease of pore fouling and enhanced backwashing efficiency but it is a function of the shear stress [13]. Several researches have studied the retention of NPs by microfiltration (MF) membrane to identify fouling mechanisms occurring during the filtration. Henry and Brant [14] showed that the cake filtration model describes the membrane fouling by nanoparticles with hydrodynamic diameter of 91 nm. However, they also indicated that, under unfavourable deposition conditions (pH, ionic strength, ratio between nanoparticle and pore diameters or the interfacial conditions), NPs could pass through and be deposited within the MF membrane structure, leading to a standard pore blocking, at least during the initial stages of membrane fouling. This result was confirmed by Trzaskus et al. [15] who described MF membrane fouling by five consecutive fouling stages: adsorption, unrestricted transport through pores, pore blocking, cake filtration and cake maturation. Trzaskus et al. [16] showed, by filtering NPs from 10 to 100 nm in a monodisperse or polydisperse sample, that the larger the NPs, the faster blockage by cake filtration occurs. It was proved that some settings of the filtration (molecular weight, concentration of steric stabilizer and filtration pressure) have a significant influence on pore blockage and cake filtration [17]. Finally, the retention efficiency and retention mechanism may be affected by adsorption phenomenon, electrostatic interactions or other interactions.

In fact, particles smaller than membrane pore size can be retained by membrane [9] and the presence of salts, pH and the valence of the cation strongly influence nanoparticles properties. It will also influence interactions between NPs or with the membrane and, therefore, the occurrence and character of the fouling stages [15]. By contrast, the NPs feeding concentration of NPs does not have any influence on the occurrence of the fouling stages, only on their establishment velocity. In fact, Trzaskus et al. [15] have shown that the filtration resistance is a function of the accumulated mass.

For UF, it was proved that the retention of NPs is clearly transmembrane pressure (TMP) dependent [18] from 60% at a TPM of 0.05 bar to less than 40% at TPM = 0.4 bar. In the same way, Wu et al. [19] showed that Quantum Dots (QD) with size of 1.5 nm, 2.2 nm, 3.2 nm and 3.8 nm are retained at 75%, 90%, 85% and 98%, respectively, by a 30 kDa UF membrane at TMP = 0.6 bar, against 10%, 20%, 45% and 70%, respectively, at TMP = 2 bar. NPs penetration profiles presented by Wu et al. [19] are also dependent of NPs size vs. MWCO.

The aim of this study is to establish an accurate and reliable methodology allowing to clearly identify the retention of NPs and the position of fouling on/in multichannel hollow fiber UF membrane. The influence of NPs size, transmembrane pressure and volume concentration factor on retention rate, fouling establishment or location of fouling was investigated. TMP applied during this study are low pressures similar to those used in drinking water treatment plant.

2. Materials and methods

2.1. Membranes

Multichannel (7 channels) polymeric hollow fiber UF membranes (ALTEON™ I, SUEZ Aquasource®, France), made of hydrophilic polyethersulfone (PES), were used in this study. They present a 200 kDa molecular weight cut-off (MWCO) with an average nominal pore size of 20 nm. The inner diameter of a channel is 0.9 mm and the external diameter of the hollow fiber is 4 mm. Filtration experiments were realized for a length of 20 cm.

These membranes allow internal-external filtration and have an average permeability of 1050 $L.h^{-1}.m^{-2}.bar^{-1}$ with a standard deviation of 50 $L.h^{-1}.m^{-2}.bar^{-1}$. Under filtration conditions, at neutral pH (7 ± 0.5), the membrane zeta potential is about -22 mV (constructor data). It is, therefore, of the same sign and intensity as the NP suspensions (see Table 1). This indicates a low probability of NP adsorption due to the repulsion forces between particles and membrane material.

2.2. Nanoparticles

In keeping with the pore size, three NPs sizes were used, a smaller (1.5 nm), a bigger (100 nm) than the membrane pore size and one close to the membrane pore size (10 nm). The silica nanoparticles used (Sicastar Red-F, Micromod Partikeltechnologie GmbH, Germany) are spherical silica NPs with diameters of 10 nm (NP-10) and 100 nm (NP-100), as are shown in Figure 1. They are labeled with rhodamine, a fluorescent dye, covalently bound in the silica matrix. To ensure that rhodamine labeling does not affect NPs adsorption and retention, a preliminary experiment with addition of 50 mmol of NaCl in feed suspension was realized. Results have shown no variation in terms of flux and retention compared to filtration without salt.

Polydispersity and shape of silica NP were checked by scanning electron microscopy (SEM) imaging. The absorption spectra were obtained for each NPs size with a spectrophotometer (UV-VIS photoLab® 6600, WTW GmbH, Germany). NPs show an absorption peak from 500 nm to 600 nm, which makes it possible to excite them with a green laser of 532 nm during Confocal Laser Scanning Microscopy (CLSM) analysis.

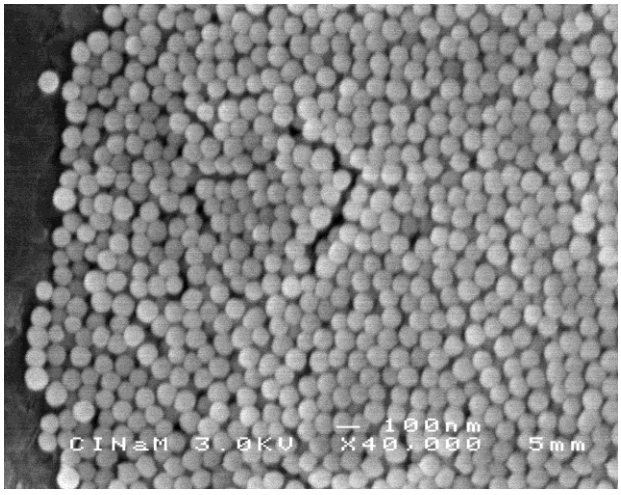

Fig. 1. SEM characterization of NP-100

Nanoparticles have hydrophilic surface with Si-OH end groups. Size distributions were obtained with Zetasizer Nano S (Malvern, England) and with individual monitoring particle analyzer NanoSight NS300 (Malvern, England) based on Nanoparticle Tracking Analysis (NTA). All measurements were performed at 20°C. Results have shown that NPs of 10 nm used in this study present an average size of 8.7 nm ± 6.6 nm for a median size of 7.5 nm and that 100 nm NPs present an average size of 100.7 nm ± 40.0 nm for a median 96.9 nm, for a total of about 30,000 particles analyzed for each size.

Smallest NPs, hydrophilic CdTe QDs (powders) coated with a proprietary mixture of low-molecular weight thiocarboxylic acid (PlasmaChem GmbH, Germany) were used to prepare suspensions to be filtered. CdTe QDs, which can be excited with a 405 nm laser and which present a maximum emission wavelength at $\lambda = 510 \pm 5$ nm (CdTe-510) were investigated in this study. This corresponds to a QDs size of 1.53 nm (NP-1.5). Zeta potential of NP suspensions were measured with a Zetasizer Nano ZS (Malvern, England).

Three different suspensions are prepared, one for each size of NP. The concentration of these three suspensions is high (see Table 1) and a dilution is necessary before analysis, to take into account the apparatus measurement range (respectively about 10^{12}, 10^{11} and 10^{8} $part.mL^{-1}$ for NP-1.5, NP-10 and NP-100). The concentration error for fluorimeter and NTA for NP-100 is respectively 2.2% and 1.6%. Neutral pH was checked for the zeta potential measurement. The main characteristics of NPs suspensions are summarized in Table 1.

Finally, NPs used are composed of solid and structured materials (CdTe and silica). They are, therefore, incompressible and keep their shape under different operating conditions. The size of NPs will be the only reason why they pass through the membrane. Considering the zeta potential of NP suspensions (close to or greater than -30 mV), and the fact that only NP are present in suspensions, the aggregation phenomenon is negligible.

Table 1
Physicochemical characteristics of NPs used in suspensions.

Parameter	NP-1.5	NP-10	NP-100
Diameter (nm)	1.53*	13.51**	100.7***
Wavelength (nm) (maximum ± 5 nm)[a]	510	585	585
Zeta potential (mV)[b]	-29.03 ± 2.03	-22.7 ± 3.54	-43.2 ± 0.85
Conductivity (µS.cm^{-1})[b]	2.7 ± 0.4	1.5 ± 0. 3	12.1 ± 0.5
Feed concentration (part/mL)	9.7x10^{13} ± 8.0x10^{13}	8.7x10^{11} ± 4.2x10^{11}	1.3x10^{12} ± 8.0x10^{11}
pH	6.86 ± 0.15	7.01 ± 0.10	6.93 ± 0.09

* Diameters from manufacturer (http://www.plasmachem.com/download/Quantum_dots_sizes_PlasmaChem_GmbH.pdf)
** Size average measured by Zetasizer Nano S
*** Size average measured by NanoSight NS300
[a] Detection ranges of emission wavelengths given by manufacturer
[b] Zeta potential and conductivity values measured by Zetasizer Nano ZS

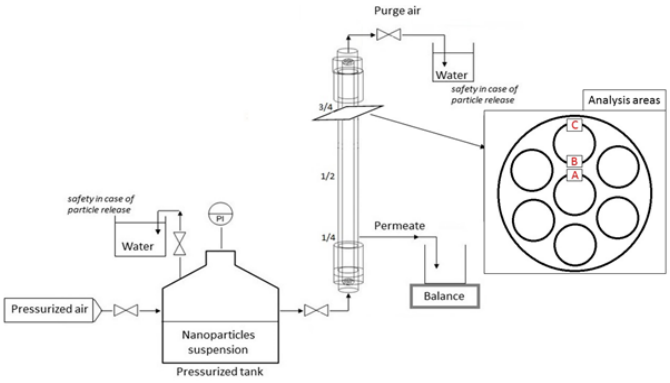

Fig. 2. NPs suspensions dead-end ultrafiltration.

2.3. Filtration experiments

Membrane module was made by potting, in an epoxy plug at each end of the module, one multichannel membrane into an external shell (PVC). For each experiment, a new module/membrane was used. Membranes were flushed with Milli-Q water (conductivity of 0.8 µS.cm^{-1}) under 1 bar of TMP to remove residues of the glycerin used for preservation of membranes. All filtration experiments were performed in vertical dead-end filtration mode using the lab-scale setup presented in Figure 2. Dead-end filtration mode was used to be close to drinking water production mode.

What is more, one of the objectives of this study is to determine if the filtration is homogeneous on the entire length of the fiber and in each channel. Pure pressurized air was connected to the tank containing NPs suspension which was itself connected to the module. The feed is a suspension of NPs in Milli-Q water ultrafiltered by membrane (ALTEON™ I, SUEZ Aquasource®, France). The feed concentrations are given in Table 1. They were selected to ensure that each NPs size could be detectable by the microscopic technics and quantifiable by fluorimeter or NanoSight. Dead-end filtration was carried out at different constant TMP which was recorded with a digital manometer with record function (LEO Record, KELLER, Swiss). The permeate was recorded by an electronic balance (Δm = ± 0.01 g). All experiences were carried out at room temperature (20°C ±2°C). At the end of the filtration, the membrane module was disconnected and the retentate contained in fiber channels was recovered by capillarity.

2.3.1. Flux analysis

Feed, permeate over the time and retentate at final filtration time were analyzed by fluorimeter (Jenway 6300, Bibby Scientific Limited, UK) and NTA for NP-100 to determine their concentration. The permeate collection beaker was wrapped with aluminum foil paper to minimize fluorescence fading of NPs during the filtration runs. The optimal measurement range of NTA is from 10^7 to 10^9 particles.mL^{-1}: solutions were diluted for analysis purposes when necessary. The aggregation, which could be the cause of a greater retention, was controlled by comparing NPs size in feed and retentate. The filtration was carried out until a different volume concentration factor reached values between 200 and 800, consistent with VCF usually used in the drinking water production plants.

The retentate was collected at the end of the filtration experiment by capillarity and analyzed to calculate the recovery rate [19]. The fouled membrane was recovered after filtration experiment and dried in a desiccator with anhydrous calcium sulfate. Then, the membrane was cut after wetting in the liquid nitrogen in order to limit the deformation of the membrane material. The fracture was performed at different lengths of the hollow fiber: ¼ - ½ - ¾ (see Figure 2) to obtain significant results and the edges of membranes obtained were analyzed with CLSM and SEM.

2.3.2. Estimation of NPs number on the membrane surface

When NPs are retained on the membrane surface, the cake thickness was estimated. Assuming that NPs are uniformly retained on the membrane surface and assuming that the distance between two particles centers is linear and equal to a NP diameter, it is possible to estimate the maximum deposition thickness over the whole membrane surface, on the 7 channels by calculating the number of NPs layers deposited.

2.4. Membrane autopsy by SEM and CLSM

Confocal laser scanning microscopy (CLSM) was used in addition to scanning electron microscopy to detect presence of fluorescent NPs on membrane surface and/or in membrane support. After filtration, fouled membranes were analyzed on their section by SEM (JSM-6320F, JEOL) at three different magnifications (x25, x75 and x400) under 3 kV with a SEI detector for magnifications of x25 and x75 and SEI detector for magnification of x400.

The tuning allowed the visualization of NPs on membrane surface at different zones and length of the fiber and allowed to determine the deposit thickness on membrane surface with the measurement tool of Image J. The thickness found was compared with CLSM results and the cake thickness estimation. Membranes fouled by fluorescent NPs were also analyzed by CLSM (TCS SP5, Leica Microsystems CMS GmbH, Germany).

For each filtration experiment, the membrane was analyzed at different lengths on its section. Two scans were made in different conditions: in a visible mode to probe membrane structure and in a fluorescent mode to reveal NPs signal. Membrane was analyzed in different areas of interest (see Figure 2). The great interest and novelty compared to previous studies is the direct analysis of the membrane section against the scan according to the depth [19]. The lateral resolution of CSLM is greater than the axial one, and allows a high accuracy of measurement: 538.16 nm instead of 5 000 nm. For the largest NPs, the excitation laser used for both scans is a green laser with a wavelength of 532 nm to best excite the NPs used. During the visible scan, the RT 30/70 separator was used and the detection of the emission was carried out over a wavelength ranging from 530 nm to 535 nm, making it possible to consider only the reflected light and, therefore, to carry out a scanning representing the visible one. For fluorescence analysis, a DD 405/532 separator filtering the excitation wavelength, and recovery of the emission signal was performed over the 575-585 nm interval.

For the smallest NPs, the excitation laser used for both scans was a blue argon laser with a wavelength of 488 nm to best excite the CdTe-510 used. During the visible scanning, the RT 30/70 separator and the detection of the emission was carried out over a wavelength ranging from 485 nm to 495 nm. For the fluorescence analysis, a DD 488/605 separator was used, and the recovery of the emission signal was carried out over the range 505-515 nm.

2.5. Fouling models

Trzaskus et al. [16] showed that rejection of NPs smaller than membrane pore size was possible thanks to combination of pore blocking and/or concentration polarization phenomena during filtration. They showed that during the dead-end microfiltration of stable NPs suspension, fouling developed in five stages (e.g. 1- nanoparticles adsorption onto the membrane, 2- transport through the membrane pores, 3- pore blocking, 4- cake filtration and 5- cake maturation) when membrane pores are much larger than NPs diameter.

Tracking the flux decline during filtration time allows to evaluate the fouling induced by NPs. During the filtration of a fluid charged with particles, the resistance is modified by the accumulation of material on the membrane surface or in the membrane depth. The study of the variation of normalized permeate flux (J / J_0) as a function of time during filtration at constant pressure allows to identify the fouling mechanism from Hermia models [20] that occurs during the filtration of suspensions or during a part of the filtration [19].

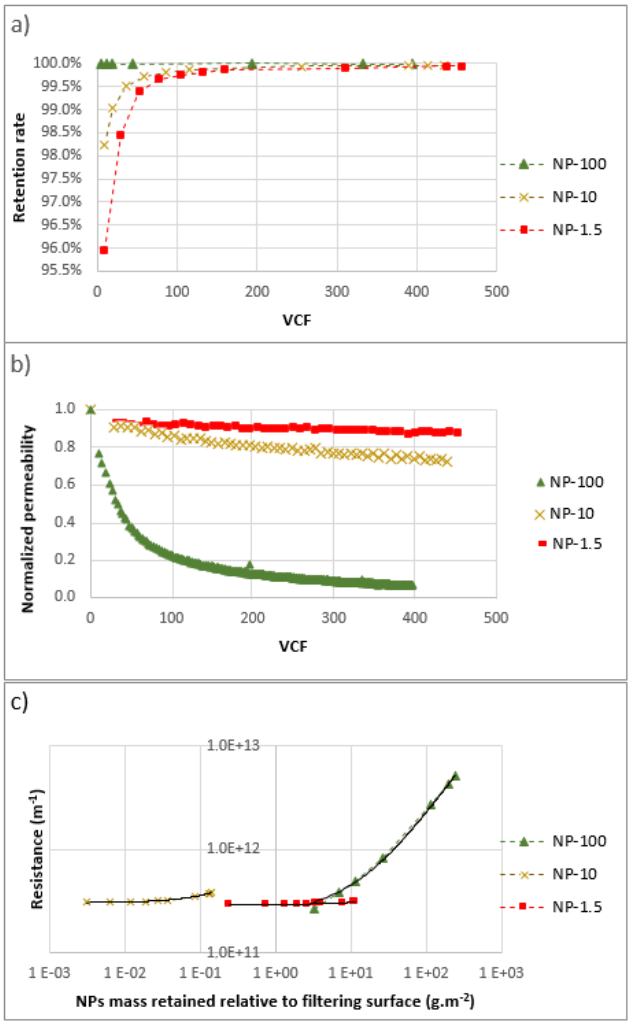

Fig. 3. a) Permeability decrease, b) theoretical retention rate as a function of volume concentration factor achieved for different NPs size and c) total resistance relative to accumulated NPs mass by m^2 of filtration surface [TMP = 0.3 bar].

3. Results and discussion

3.1. Influence of NPs size on retention

3.1.1. Retention of NPs

Whatever the TMP applied or the VCF achieved, final retention rates calculated from concentrations of retentate and permeate collected and analyzed at the end of the filtration are greater than or equal to 99.9% for NP-100, greater than 99% for NP-10 and are between 77.7% and 92.8% for NP-1.5. Permeates were also collected over the filtration time and concentrations of each sample were determined, which allowed theoretical retention rates over the filtration time to be calculated by mass balance. These theoretical retention rates, presented in Figure 3a, are overestimated because NPs blocked in and/or on membrane, and therefore not recovered in the retentate, are not considered. It appears that at least 99.9% of NP-100 are retained from the start of the experiment while retention rates of NP-10 and NP-1.5 increase with the filtration time.

The fouling of the membrane during the first steps of the experiment explains this retention rate increase which is directly linked to the membrane permeability decrease [16]. Figure 3b shows that the filtration of smallest NP-1,5 does not induce an important permeability decrease (not superiors to 20% in the conditions studied) even if they are retained by the membrane after few minutes of filtration. The permeability decrease induced by the medium NP-10 (close to pores diameter), is more important and increases with the VCF and, therefore, with the accumulation of NP-10 on/in the membrane. It reaches about 40% in maximum operating conditions tested (TMP = 0.4 bar; VCF 800). As shown in Figure 3a, the retention rate of NP-10 increases with the VCF which explains that the permeability decreases progressively like for NP-1.5. However, for the largest NP-100, retention had been total since the start of the filtration and that induced a strongly permeability decrease at the beginning of the filtration experiment until VCF of 100. From VCF 100 to 300, the permeability decreases slowly to reach a permeability decrease value superior to 90%. After an approximate VCF of400, the shape of permeability curve decrease is very low which indicates that the retention of NP-100 has lower impact on permeability.

3.1.2. Recovery of NPs

Recovery rate is defined as the percentage of NPs recovered in the permeate and the retentate relative to the number of filtered NPs. Recovery was determined to evaluate if NPs were retained based on the size exclusion alone or if they were adsorbed on the membrane surface and/or trapped in the membrane pores. High recovery is expected for NPs larger than membrane pores resulting in size exclusion or for smallest NPs vs. the pore size which allows nanoparticle transport through the membrane without rejection. Low recovery is expected when a considerable fraction of NPs were retained inside the membranes [19].

Results obtained show that NP-10 present a greater recovery rate than NP-1.5 and NP-100. The low recovery can be explained based on this fact that NP-1.5 pass through the membrane and remain blocked in the membrane while NP-100 are stopped on the surface of the membrane and make a cake layer which stays in place at the end of the filtration (see Figure 4). This means that NP-100 are not recovered in the retentate.

The recovery rate is calculated using the final concentrations of retentate and permeate. By mass balance, it is then possible to estimate the number of NPs recovered in the retentate, in the permeate and those that remained blocked in the membrane support and/or on the membrane surface. This allows the repartition of NPs at the end of the filtration to be studied. All these values were compared to the total number of NPs engaged during the filtration as reflected in Figure 5. Results show that about 20% of smallest NP-1.5 filtered pass through the membrane and they are recovered in the permeate side against about 10% of NP-10 and lower than 2% of largest NP-100. Repartition of NPs obtained shows that only 3% of NP-1.5 smaller than membrane pore size are recovered in the retentate, the retention made by blocking of NPs in/on membrane is the largest part. Trzaskus et al. obtained similar results for identical pore size / NP size ratio around one log: pore clogging and nanoparticle deposition later on leads to the formation of a secondary membrane, which limits NP transport. Concerning NP-100, larger than the membrane pore size, a low recovery is obtained in the retentate and more than 85% of NPs filtered are blocked on membrane. The blocking of NP-100 is mainly made by a cake on the membrane surface as is shown in Figure 4 a-c, and a low penetration of NP-100, of about 20 µm in depth, have been visualized by CLSM in membrane support. Finally, NPs with size close to membrane pore size are those that are the most recovered in the retentate (see Figure 5).

Figure 6 shows a retention of NP-10 forming a tight cake layer on the membrane surface indicating that more NPs are recovered in the retentate. As is shown in Figure 3a with the theoretical retention rate calculated from permeate concentration over the time (i.e., collection of permeate volumes vs. time), NP-10 pass through the membrane during the first minutes of the filtration, which reveals that retention is made in the membrane, too. CLSM was used to locate NPs and therefore the fouling on and/or in the membrane. Variation of TMP did not have the same influence on global recovery rates for each NPs size (see Figure 7). For NP-1.5, the increase of TMP increases the recovery of NPs. Variation of TMP shows no significant modification of NP-10 recovery while NP-100 are less recovered with the increase of TMP.

3.1.3. Location of fouling

3.1.3.1. Calculation method

The CLSM analysis of the membrane samples on their section allowed to localize the NPs and to obtain the deposit thickness on the membrane or the penetration profiles in the membrane. The image obtained with CLSM is composed of two scans: one scan in reflective mode imaging only the membrane to determine the membrane surface position and one in fluorescent mode imaging the NPs fluorescent signal (see Figure 6). Image analysis was performed using the software Image J 1.43 (National Institutes of Health, USA). The images obtained by CLSM are formed of 512 × 512 pixels. Presence detection and distribution profiles of NPs were exactly located at the same position on the visible and fluorescent scans in order to analyze the NPs distribution profile relative to the membrane surface. The maximum of the first peak in the visible scan is defined as the membrane surface and the associated pixel is attributed a value of zero. The resulting graphic provides the distribution profile of nanoparticles relative to the membrane surface.

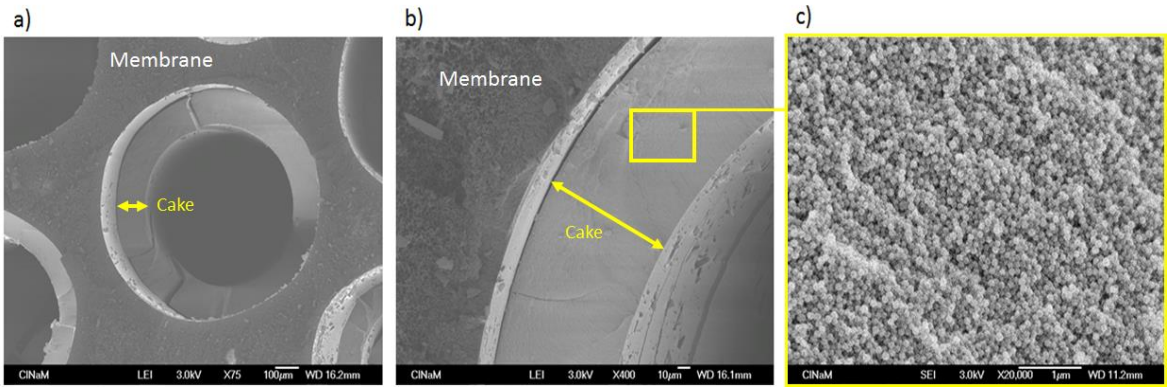

Fig. 4. SEM imaging of NP-100 deposit on membrane surface after filtration of NP-100 suspension [TMP = 0.2 bar; VCF = 500]- at different magnifications a) x75 b) x400 and c) x20 000.

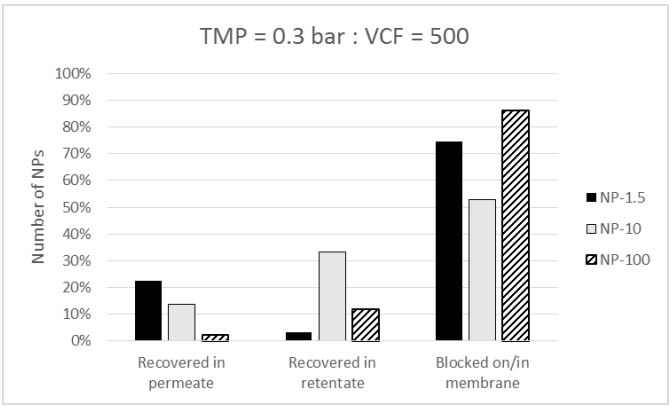

Fig. 5. Repartition of NPs at the end of the filtration (in number).

The deposit thickness, if there is a deposit, can be estimated as the full width at half maximum. An eventual depth of NP penetration in membrane can also be identified by a fluorescent intensity higher than the baseline (corresponding to the estimated noise level) inside the material. The penetration depth is defined like the distance relative to the membrane surface for which the intensity average of three consecutive pixels is higher than the baseline. To estimate the baseline, a clean membrane, which had been rinsed with ultrapure water, was analyzed in a fluorescent scan with the same analysis parameters than those employed for the fouled membrane. More than fifty measurements were realized along the fiber showing homogeneity of NPs penetration.

3.1.3.2. Distribution profiles

As shown in Figure 8, the fluorescent signal indicates the presence of NPs throughout the membrane for NP-1.5 (see Figure 8a) which confirms the passage of NPs through the membrane during the filtration and the in-depth fouling of the membrane. Fluorescent signal is obtained on the membrane surface, reflecting a NP-1,5 deposit. NP-10 (Figure 8b), penetrate up to a thickness close to 50 µm, which corresponds to the skin of the membrane. A tight deposit on the surface of the membrane is also identified which indicates that two fouling mechanisms can be envisaged: an in-depth fouling and a cake filtration.

Finally, for the NP-100 (see Figure 8c), a large surface deposit is observed, explaining the strong decrease of the permeability and showing a cake filtration fouling mechanism. Moreover, a little penetration over about 20 µm has been identified in the membrane material.

3.1.4. Fouling mechanisms

The main fouling mechanism(s) operating during filtration can be determined by comparing the experimental values of permeate flow rates with models proposed by Hermia [20]. In this study, high feed concentration was used, which made identification of each stage advanced by Trzaskus et al. [16] complicated. The identified mechanisms do not vary with the TMP applied or the VCF achieved for each size of NPs. The results show that permeability decreases during the filtration of NP-100 suspension is due to a cake filtration fouling model (R^2 = 0.99) (see Figure 9a). At the beginning of the filtration, during the first 50 mL of filtered permeate, complete blocking is the best description of the flux decline (R^2 = 0.98). This result confirms the retention rate superior to 99.9% observed from the beginning of the filtration and the penetration profile obtained by CLSM. In fact, the complete blocking identified at the beginning of the filtration reflects the low penetration of NP-100 in membrane material identified by CLSM. The model of cake filtration followed by standard blocking best describes the flux decline observed during NP-10 filtration (R^2 > 0.99) (see Figure 9b).

Intermediate pore blocking and complete blocking show lower R^2 close to 0.5, which explains why these two models have been neglected for NP-10 filtration. Because the size of the NP-10 is close to that of the membrane pore, an estimation can be made that the NP-10 follows a standard blocking model before the formation of a surface deposit and the subsequent observation of the cake filtration model for remainder of the experiment (see Figure 9b). These both models found are confirmed by the increase of retention rate during the filtration time (see Figure 3a) and the penetration profile obtained which reflects a NP-10 location on the membrane skin and a cake layer on the membrane surface (see Figure 8b).

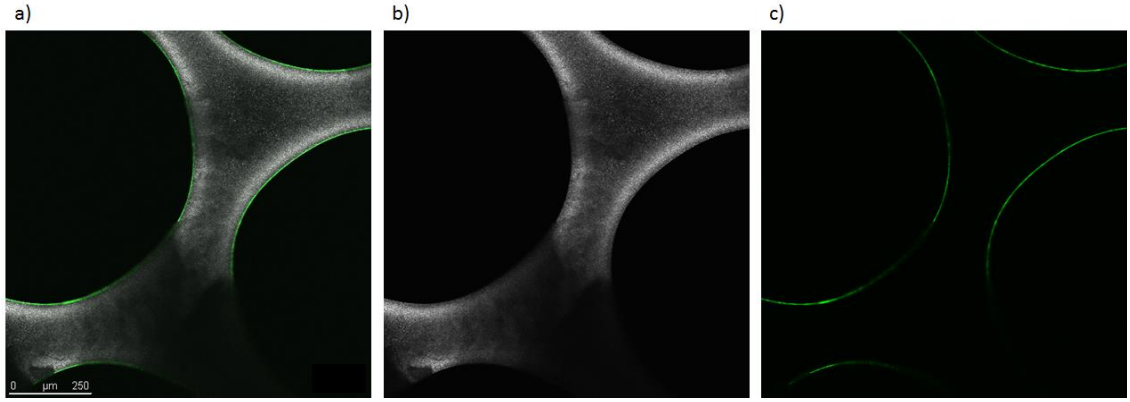

Fig. 6. CLSM imaging of membrane after filtration of NP-10 suspension [TMP = 0.2 bar; VCF = 500] – a) overlays of scans, b) membrane scan in reflective mode and c) NPs scan in fluorescent mode.

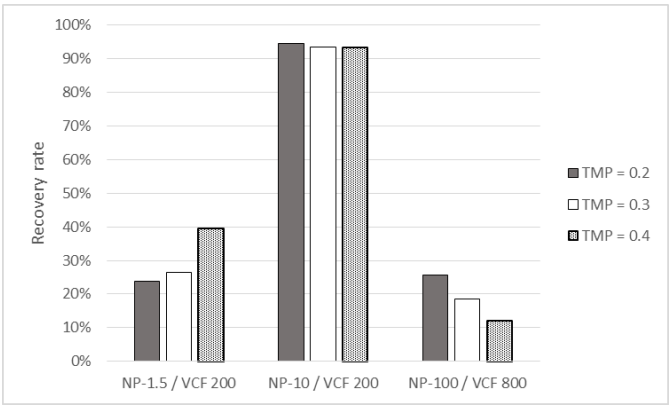

Fig. 7. Variation of recovery rate as function of operating conditions (NP sizes and VCF) for different TMP.

Finally, the application of Hermia models had to be decomposed over the filtration experiment to ensure consistency with experimental data gathered during NP-1.5 filtration. A standard blocking model seems to better describe the permeability decrease observed during the first steps of NP-1.5 filtration, during the passage from 20 to 110 mL of permeate corresponding to a filtration time of 60 to 260s (see Figure 9c). Intermediate and complete blocking have been tested on the same sections and shows $R^2 < 0.3$ with experimental data. However, before 60s of filtration, no model accounts for the observed flux behaviour. After the filtration of 110 mL of permeate (t = 260s), the data from the experiment follows a cake filtration model reflecting the formation of a NP-1,5 deposit on the membrane surface. Penetration profile obtained with CLSM imaging (see Figure 8) shows that NP-1.5 are stopped in the entire membrane material and that a fluorescent signal is obtained on the membrane surface, reflecting the presence of NPs deposit (see Figure 10a). It therefore appears that results obtained with the Hermia models and the microscopic observations are consistent.

These experiments are realized considering the feed concentration of NPs in number. The final accumulated mass is therefore not the same for the different NPs sizes. Figure 3c shows the variation of the resistance as a function of the mass stopped by square meters. For NP-1.5, the accumulated mass is small as is the resistance. Moreover, the variation of resistance vs. mass is also limited. Similar results are obtained for NP-10 but the variation is doubled. For NP-100, the accumulated mass is important and the resistance of the cake strongly increases vs. mass. For the same resistance, the accumulated mass is lower for NP-1.5 (NP penetration in the membrane) and NP-10 (penetration in the skin and accumulation) meaning that the fouling model involved is more constraining than for NP-100 (cake filtration). The process parameters (i.e., flux and retention), the CLSM penetration profiles and the modelling are therefore all consistent with one another.

3.2. Influence of TMP

The influence of the TMP variation on different parameters has been studied, for example, on retention rate, on recovery rate and on repartition of NPs relative to the membrane surface. Results of deposit thicknesses values on the membrane surface measured by CLSM and SEM are consistent when the microscopic resolution is sufficient to visualize the cake (see Figure 11). The variations can be explained by the locations of microscopic analysis which are not exactly the same. However, thicknesses found by the mass balance taking into account the recovery rate is greater than the deposit measured. In fact, deposit thicknesses obtained by mass balance are calculated assuming that NPs stopped are all retained on the membrane surface, uniformly.

*3.2.1. NP-100_*

Variation of TMP has no impact on NP-100 retention as it is shown in Figure 12a. NP-100 retention rate is always superior or equal to 99.9% all along the filtration experiment. However, the permeability declines do not follow the same shape in function of the pressure applied and it appears that the increase of TMP induces a more acute drop in permeability for a same feed volume filtered, which would lead to believe that a modification of cake structure could be expected.

The permeability decline is drastic during the first time of filtration (cf. part 3.1.1). Thus, if the filtration experiment is conduced until a low VCF, the TMP has an influence on the final permeability value because the slope is a function of the TMP. However, if a high VCF is achieved, superior to 600, the variation of the final permeability does not appear to be significantly linked to the TMP applied (see Figure 12). By applying fouling models to experimental data of permeability, it is possible to obtain the blocking constant relative to the cake filtration, k_{cf}, used in the Hermia models. At constant VCF, K_{cf}, decreases with the increase of TMP. This constant is linked to the specific cake resistance which can be calculated with the following equation [21]:

$$k_{cf} = \frac{\alpha X \mu}{A^2 TMP_0} \quad (1)$$

where α is the specific cake resistance (m.kg^{-1}), X is the NPs concentration (kg.m^{-3}), μ is the dynamic viscosity of the permeate (Pa.s), A is the membrane surface, considered as a constant over the time (m^2), and TMP_0 is the transmembrane pressure applied (Pa). This specific cake resistance was multiplied by the NPs mass stayed blocked on the membrane for each filtration experiments used to evaluate the cake characteristics. For a fixed value of VCF achieved of 800, the resistance induced by deposit of NPs relative to mass deposited increases from 2.6×10^{11} to 3.6×10^{11} and 5.2×10^{11} m for a TMP of 0.2, 0.3 and 0.4 bar applied during filtration, respectively. This resistance is linked to the mass stopped which composes the cake layer on the surface of the membrane. That is why the investigation of deposit thickness was realized by SEM and CLSM visualization.

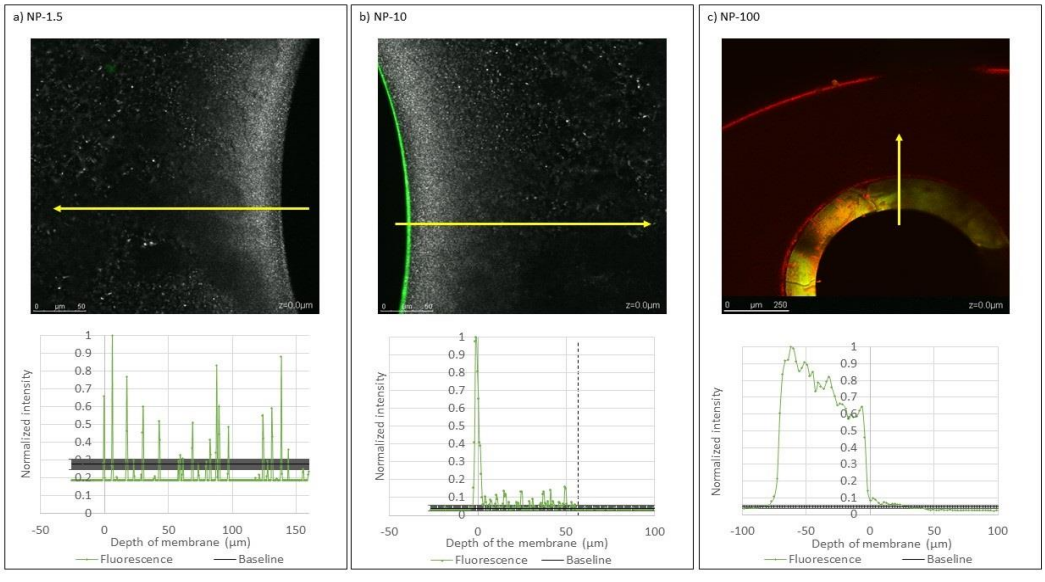

Fig. 8. Distribution profiles relative to membrane surface obtained with ImageJ treatment of CLSM image after filtration of a) NP-1.5 suspension, b) NP-10 suspension and c) NP-100 suspension [TMP = 0.3 bar; VCF 500].

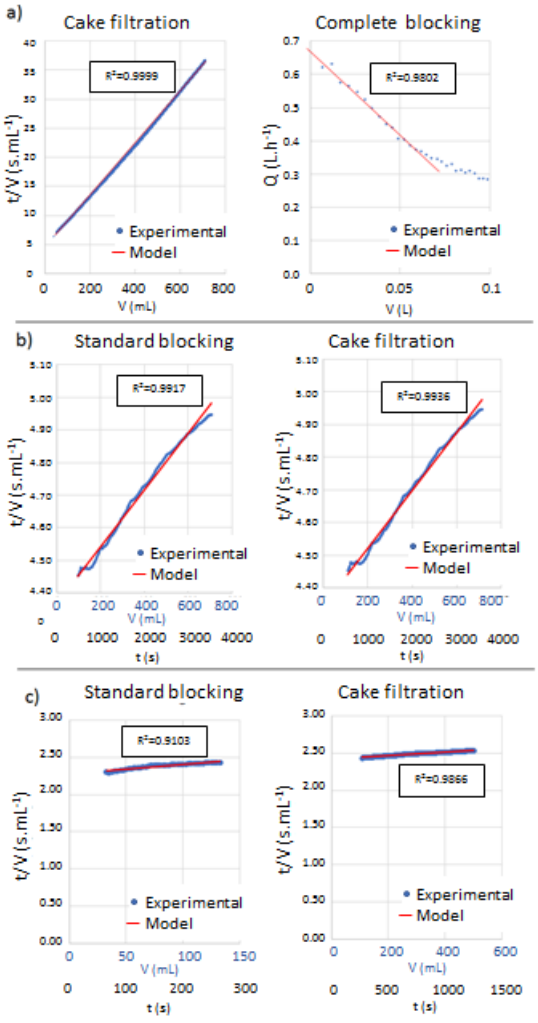

Fig. 9. Fouling models found for NPs filtrations of a) NP-100, b) NP-10 and c) d) NP-1.5 [TMP = 0.3 bar; VCF 500].

At constant VCF, the influence of TMP on the percentage of NP-100 that remained blocked on the membrane has been studied. The results presented in Figure 12a are valid for a VCF of 800, noting that the percentages proposed here are relative to the number of NPs recovered in each flux relative to the number of filtered NPs. When the TMP increases, the NP-100 recovered in the permeate and in the retentate decrease which increases the quantity of NPs blocked on membrane. The explanation is that a cake layer is formed quickly at high TMP and the cake structure is more compact: when the TMP increases less NPs are recovered in the retentate but stay blocked in the cake layer. The distribution profiles of NP-100 show a very small penetration of NP-100 in the membrane. No notable variation of the measured penetration depths in function of the TMP applied was found. The penetration is weak due to the large size of NP (vs. pore size), from 21 µm to 30 µm, with smallest penetration for a low pressure, from 21 µm to 26 µm. These values are lower than that of the thickness of the membrane skin, i.e., 50 µm.

3.2.2. NP-10

As is shown by Figure 12b, the increase of TMP for the filtration of NP-10 suspension seems to have an impact on the retention and the permeability. At TMP = 0.2 bar, the retention of NP-10 is rapidly efficient which induces that the permeability decrease is faster and more important than at TMP = 0.3 or 0.4 bar. A more important pressure forces the NP-10 to pass through the membrane. However, the minimum retention rate observed, at the beginning at the filtration, is never lower than 97% and an achievement rate of 99% is obtained after a VCF of 40 for each case. These results explain the final retention rate, superior or equal to 99.9%. Differences between permeabilities observed can be explained by the change of recovery rate, by variations of fouling characteristics (i.e., duration, constants) and by variation of the fouling location in function of TMP applied.

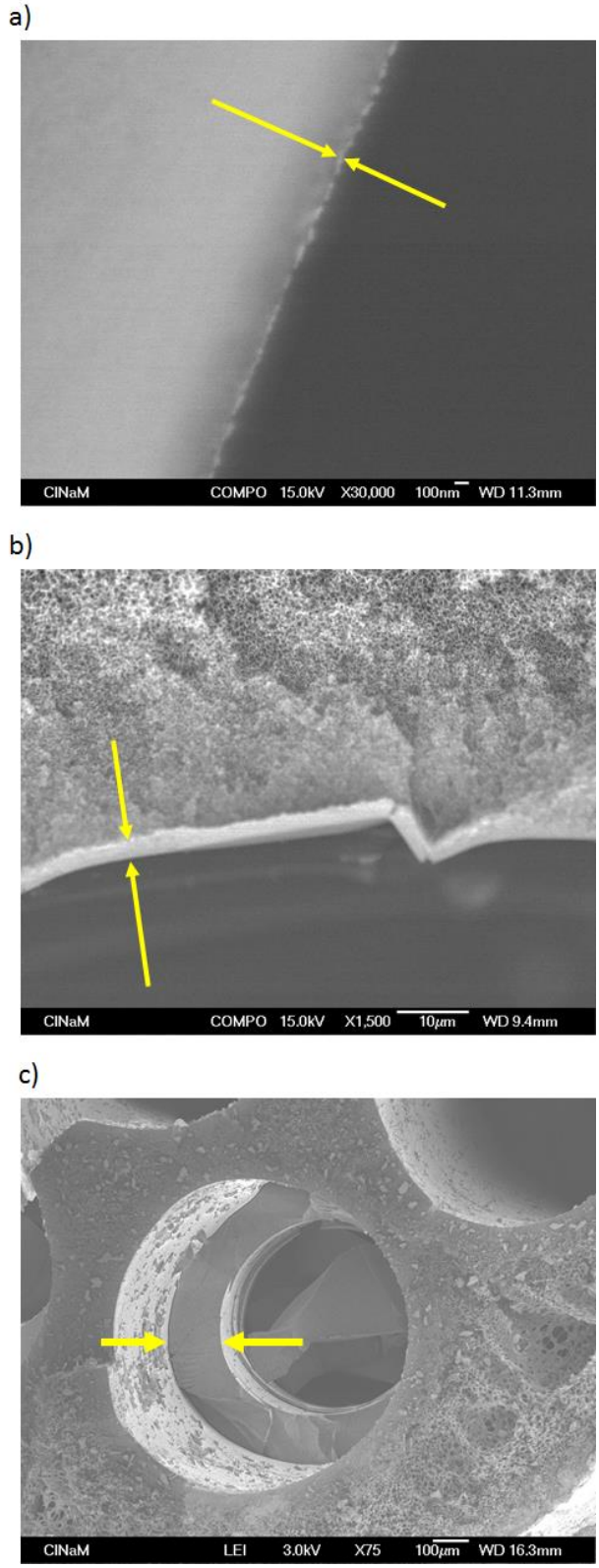

Fig. 10. Surface deposit of a) NP-1.5, b) NP-10 and c) NP-100 on membrane surface after filtration [TMP = 0.4 bar; VCF = 800].

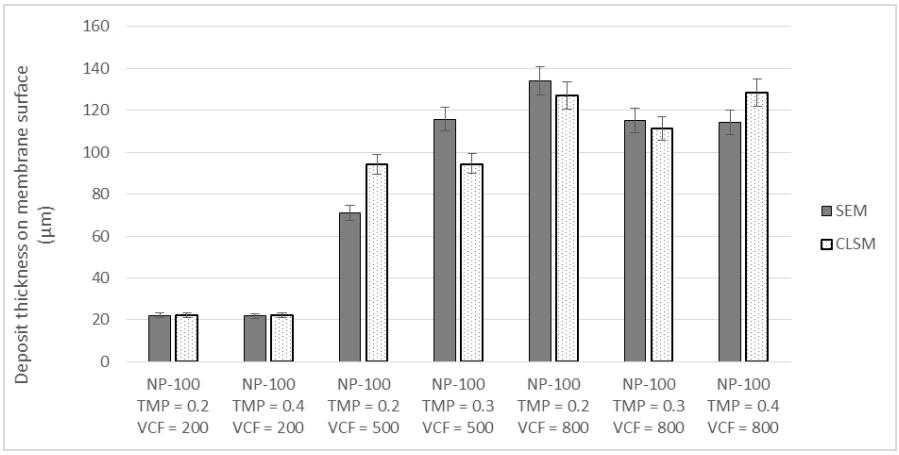

Fig. 11. Comparison of NP-100 deposit thicknesses on membrane surface found by microscopic techniques.

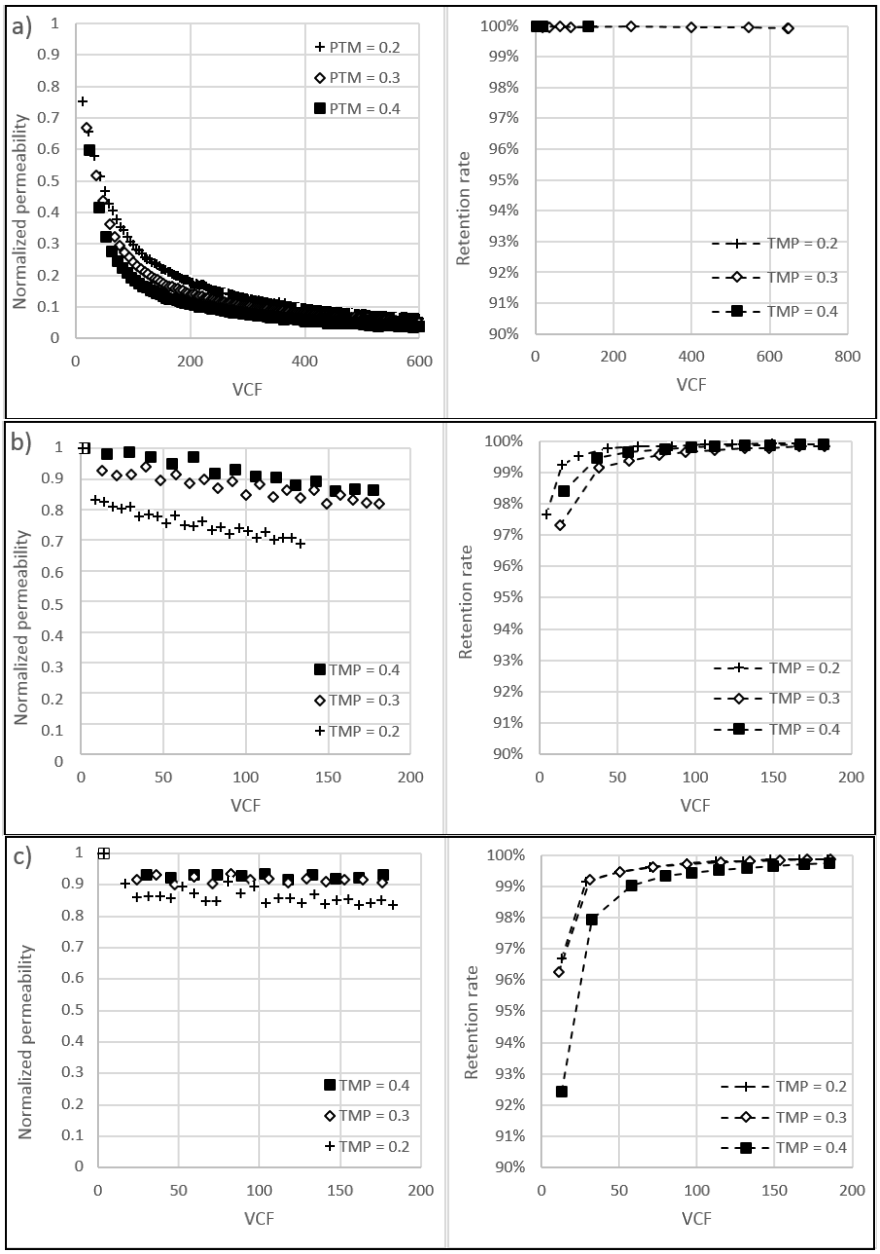

Fig. 12. Effect of TMP on permeability decline and retention rate of a) NP-100, b) NP-10 and c) NP-1.5.

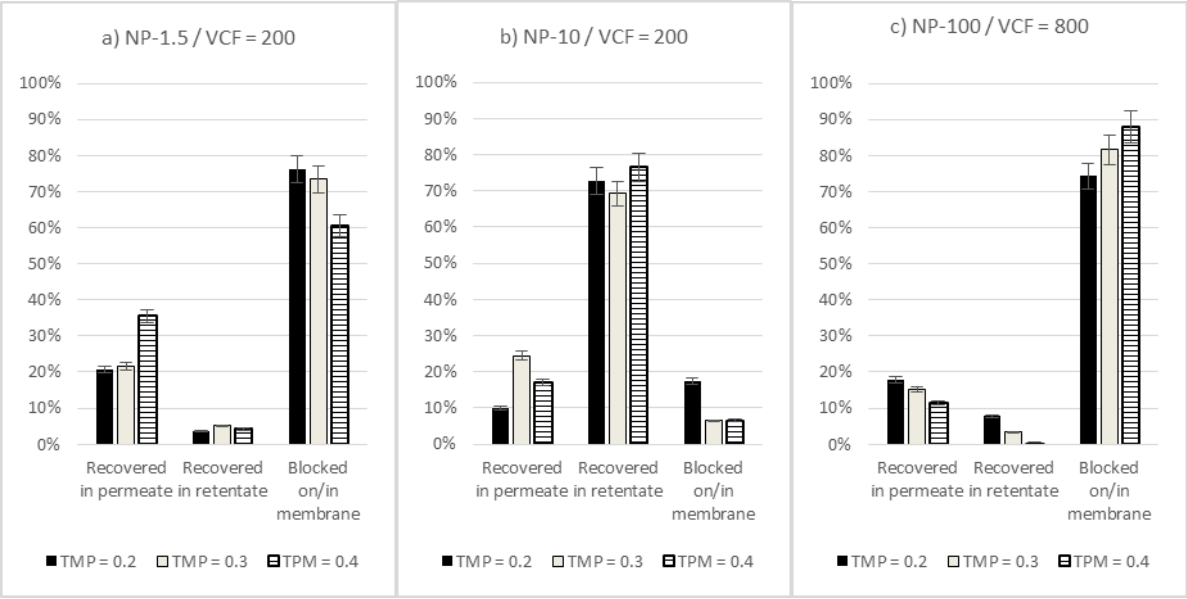

Fig. 13. Percentage of NPs recovered in the permeate, recovered in the retentate and blocked on and/or in membrane at constant VCF for different TMP after filtration of a) NP-1.5 suspension, b) NP-10 suspension and c) NP-100 suspension.

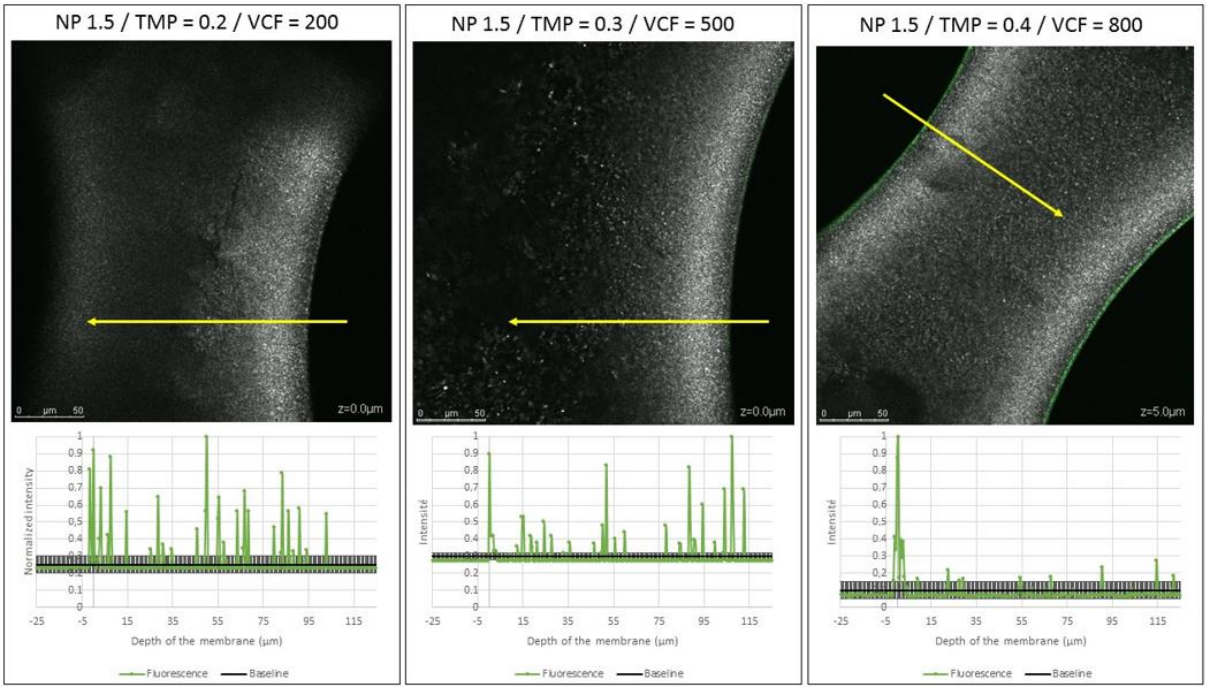

Fig. 14. Penetration profiles of NP-1.5 obtained by CLSM analysis after filtration under different conditions (TMP and VCF).

Considering the NP-10 repartition at the end of filtration (see Figure 13), the increase of TMP decreases the percentage of NPs blocked in the membrane and pushes more NPs through the membrane than at TMP = 0.2, inducing an increase of recovered NPs in the permeate. The percentage of NP-10 recovered in the retentate is important which means that NPs retained by the membrane are not blocked in a thick cake layer on membrane surface as is the case for NP-100. In fact, SEM imaging of membrane fouled by NP-10 shows a very thin deposit (see Figure 10b). CLSM images and the penetration profiles obtained show a penetration in the membrane skin which means that there should not be so many particles on the cake formed on the membrane surface. Tarabara et al. [22] studied the morphology of the cakes obtained during filtration of 30 nm NPs. They showed that a cake grows step by step. According to this study, the cake grows from the formation of a porous layer which will be rearranged more compactly once a critical thickness is reached. It is possible that the cake formed by the NP-10 on the membrane surface did not reach a sufficient thickness level. A rearrangement of NP-10 in the cake cannot occurs and the cake stability is low. NP-10 could therefore be recovered in the retentate by degradation of cake layer during collection of the retentate by capillarity. Distribution profiles of NP-10 obtained by CLSM show a narrow deposit on the membrane surface and an in-depth penetration of NPs in the membrane. Penetration depths found for NP-10 on all the experiments are between 46.5 µm and 63.5 µm into the thickness of the membrane skin (i.e., 50 µm). The only definitive conclusion that can be drawn is that, for each TMP tested, NP-10 are retained by the membrane in its skin then progressively on its surface. For each experiment, standard blocking and cake filtration were identified as the fouling mechanisms describing the better macroscopic data obtained and have been confirmed by CLSM observations.

3.2.3. NP-1.5

The increase in TMP reduces the final retention rate of NP-1.5. This result can be explained by the fact that a strong TMP pushes NPs through the membrane and the retention rate of 99% is achieved after the passage of a high permeate volume (see Figure 12c). During the filtration, the fouling of the membrane by NPs modifies the membrane retention efficiency. Considering the variations of the recovery rates in function of the applied TMP, Figure 13a confirms that passage of NP-1.5 through the membrane is more important when TMP is higher. However, the quantity of NP-1.5 recovered in the retentate does not vary significantly and the percentage of NPs blocked in the membrane decreases. A hypothesis which can be advanced is that at high pressure, a cake layer is formed. This cake formed by NP-1.5 constitutes a secondary membrane more selective than the real one and the retention improve. Clean water filtered by the cake passes through the membrane and flushes the NPs deposited on membrane support resulting in a release of NPs in the permeate. As shown in Figure 14, membrane seems to be flushed when the applied TMP is higher. This result confirms the increases of NPs quantity in the permeate observed at high TMP, as reported in Figure 13a.

3.3. Influence of VCF

3.3.1. Retention rate and permeability

The reproducibility of experiments is demonstrated by the fact that the retention rates obtained at the same TMP evolve in the same manner over the filtration time for different VCF achieved with a maximum margin of error of 5%. It should also be noted that during NP-100 filtration, VCF has no influence on the final retention rate obtained, as NP-100 have been totally retained since the beginning of the filtration (first sampling after 15 s shows a retention rate > 99.9%). However, for NPs smaller than the membrane pore size, greater final retention rates are obtained for experiments conducted until high VCF. As it is shown in Figure 3a, the theoretical retention rate increases over the filtration time for NP-10 and NP-1.5.

On the other hand, the passage of NPs occurs only during the firsts steps of the filtration, so final retention rates will be higher if the filtration is conducted over a longer period of time. Whatever the TMP applied, a theoretical retention rate of 99% is achieved after a VCF of 35 and 60 for NP-10 and NP-1.5, respectively (Figure 12b and c). Nevertheless, if the retention rate increases with filtration time, the permeability decreases in the same time. A higher VCF will therefore lead to a lower final permeability.

3.3.2. Recovery rate

As for TMP, variation of VCF does not have the same influence on the global recovery rate in function of NPs size (Figure 15). NP-1.5 are less recovered with the increase of VCF while NP-10 and NP100 seem to be less recovered at medium VCF than at low or high VCF.

Considering experiments at constant filtration pressures (see Figure 16), the influence of VCF on location of NPs can be explained. As shown previously, the retention rate of NP-1.5 and NP-10 increases with the VCF and percentage of NPs recovered in the permeate for these both NPs decrease with VCF increase. Moreover, the percentage recovered in the retentate for NP-1.5 also decrease, which shows that NP-1.5 are more retained in/on the membrane over the filtration run. Concerning NP-10, it appears that the percentage of NPs recovered in the retentate significantly decreases and percentage blocked in/on membrane is increased significantly for a variation of VCF from 200 to 500. These variations observed at TPM = 0.4 are exactly the same at TMP = 0.2.

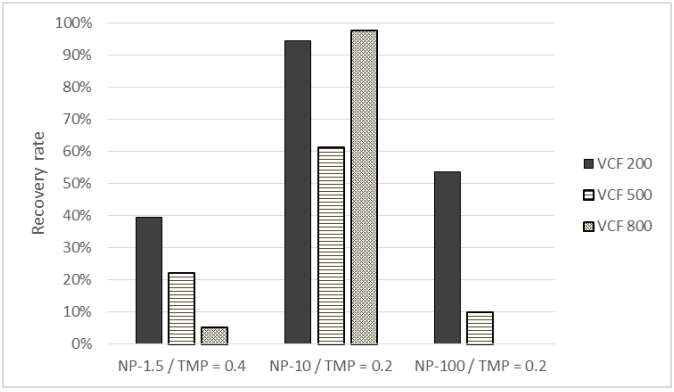

Fig. 15. Variation of recovery rate as function of operating conditions (NP sizes and TMP) for different VCF.

In better words, the increase of VCF induces that more NP-10 participate to the cake layer construction. This one is more stable and lower number of NPs are recovered in the retentate. Then from VCF of 500 to VCF of 800, an increase of NP-10 percentage recovered in the retentate and a decrease of quantity blocked in/on membrane are observed. A cake degradation during the retentate recovery at the end of the filtration or the achievement of a limit stable deposit thickness may explain the observations. For NP-100, results show that at low VCF, an important quantity of NPs are recovered in the retentate. The same explanation than for NP-10 can be made: the cake is a neither thick nor stable so a large quantity of NPs is collected with the retentate. At VCF 500, the cake layer is very thick and structured (see Figure 4). The recovery in the retentate became therefore very weak.

3.3.3. Membrane fouling

The cake layer thickness of NP-100 observed on membrane surface increases with the VCF. Figure 17 shows that a deposit thickness of 22.2 µm is found for a VCF of 200 against a deposit thickness of 70.2 µm for a VCF of 500 achieved. This result can be explained by the fact that more NPs are filtered and participate to the deposit. Deposit thicknesses found are consistent with the permeabilities observed and with the fact that the permeability becomes almost constant after VCF of 500 (see Figure 12a). The distribution profiles of NP-10 show the presence of NPs on the membrane surface and very few in the membrane skin. With the increase of VCF (VCF 800), the width of the first pic on the fluorescent profiles increases which reflects an accumulation of NP-10 on the membrane surface. In the same way, the distribution profiles of NP-1.5 show presence of NPs on membrane. At VCF of 800, a small thickness cake appears on the fluorescent profiles (see Figure 14). However, a homogeneous deposit layer thicknesses of NP-1.5 appears on the surface of the membranes. The thickness cannot be estimated due to the resolutions of CLSM and SEM.

4. Conclusions

Through this study, a methodology of accurate and reliable localization of the membrane fouling by the fluorescent NPs used as probes was developed. The use of CLSM with a membrane analysis on its section yielded penetration profiles relative to the membrane surface with an accuracy of 538.16 nm (axial resolution of CLSM under analysis conditions used) against a pitch of 5000 nm with a methodology previously developed (by Wu et al., 2014). The reliability of the results was demonstrated by the consistency obtained by the different characterization techniques used (i.e., mass balance, fouling models, microscopies). The retention potential of NPs with sizes smaller, close to and bigger than the UF hollow fiber pore size (20 nm) in ideal suspensions was studied. It was found that 100 nm NPs were all retained (retention rate ≥ 99.9%) by these membranes from the beginning of the filtration, the retention being carried out only on the membrane surface with a very low penetration thickness (some NP-100 are detected from 20 µm to 30 µm into the skin). Membrane used presents good final retention rate (> 99%) for NPs of 10 nm, the retention rate increasing with the VCF and with the membrane fouling establishment. Location of 10 nm NPs by CLSM showed presence of 10 nm NPs on the membrane surface and only in the membrane skin confirming fouling models identified with macroscopic data. Finally, it has been demonstrated that the NPs of 1.5 nm can be retained (retention rate > 77.7%) by these UF membranes, with an increase of the retention rate with the increase of VCF achieved. The increase of this retention rate can be directly related to the blocking of NPs in the total membrane material (surface, skin, support). The results also show that operating conditions do not have any influence on the fouling mechanisms established during filtration but on the characteristics obtained. It has been proved that transmembrane pressure applied during filtration may have an influence on cake structure, resistance of fouling or penetration of NPs in the membrane material. Finally, CLSM analysis in the different channels and at different lengths of the hollow fiber did not reveal any preferential filtration zones by the membrane. The filtration of mixed NP suspension is in progress and will the subject of a forthcoming paper.

Acknowledgements

The project leading to this publication has received funding from Excellence Initiative of Aix-Marseille University - A*MIDEX, a French Investissements d'Avenir programme. It has been carried out in the framework of the Labex MEC. The authors acknowledged Patrick Sauvade and Aquasource®, SUEZ, for providing membranes used during this study.

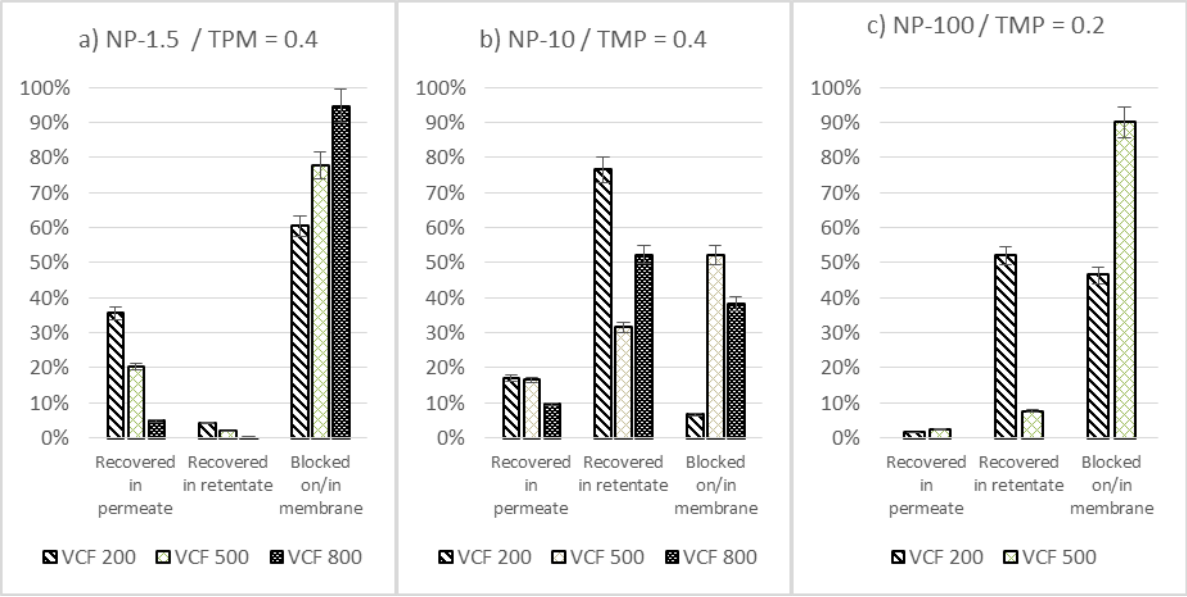

Fig. 16. Percentage of NPs recovered in the permeate, recovered in the retentate and blocked on and/or in membrane at constant TMP for different VCF after filtration of a) NP-1.5 suspension, b) NP-10 suspension and c) NP-100 suspension.

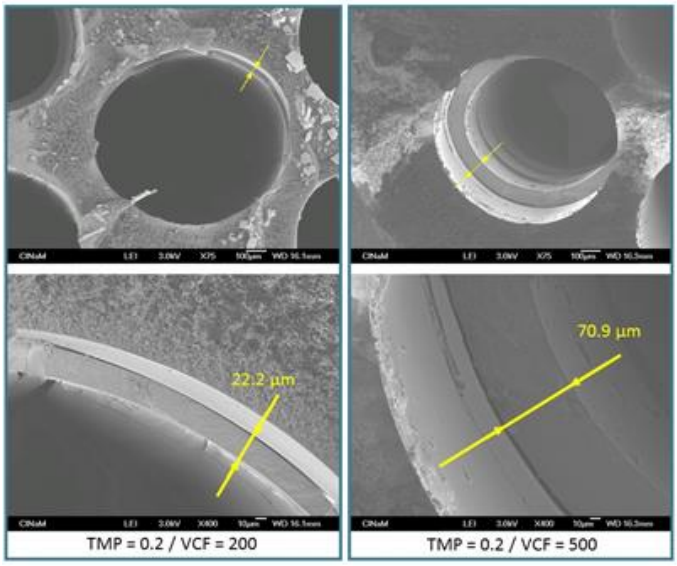

Fig. 17. SEM observation of membrane fouled by NP-100 for different VCF achieved

References

[1] F. Gottschalk, B. Nowack, The release of engineered nanomaterials to the environment, J. Environ. Monit., 13 (2011) 1145.
[2] P. Andujar, S. Lanone, P. Brochard, J. Boczkowski, Effets respiratoires des nanoparticules manufacturées, Rev. Mal. Respir., 26 (2009) 625–637.
[3] D. Palomino, Nanoparticules: Risques pour l'homme et l'environnement, GWA, 89 (2009) 979–990
[4] C. Santaella, M. Auffan, A. Thiery, J.-Y. Bottero, Reproduire un écosystème pour évaluer l'impact des nanoparticules, Biofutur, 347 (2013) 46–49.
[5] A. Simon-Deckers, Effets biologiques de nanoparticules manufacturées: influence de leurs caractéristiques, AgroParisTech, 2008.
[6] R. Hischier, T. Walser, Life cycle assessment of engineered nanomaterials: State of the art and strategies to overcome existing gaps, Sci. Total Environ., 425 (2012) 271–282.
[7] M. Troester, H.-J. Brauch, T. Hofmann, Vulnerability of drinking water supplies to engineered nanoparticles, Water Res., 96 (2016) 255–279.
[8] N. Wu, Y. Wyart, J. Rose, B. Angeletti, P. Moulin, Application of membrane processes in fractionation of elements in river water, Water Sci. Technol., 72 (2015) 2278-2291.
[9] D. A. Ladner, M. Steele, A. Weir, K. Hristovski, P. Westerhoff, Functionalized nanoparticle interactions with polymeric membranes, J. Hazard. Mater., 211 (2012) 288–295.
[10] F. Springer, S. Laborie, C. Guigui, Removal of SiO_2 nanoparticles from industry wastewaters and subsurface waters by ultrafiltration: Investigation of process efficiency, deposit properties and fouling mechanism, Sep. Purif. Technol., 108 (2013) 6–14.
[11] T.E. Abbott Chalew, G.S. Ajmani, H. Huang, K.J. Schwab, Evaluating Nanoparticle Breakthrough during Drinking Water Treatment, Environ. Health Perspect., Aug. 2013.
[12] J. Decarolis, S. Hong, J. Taylor, Fouling behavior of a pilot scale inside-out hollow fiber UF membrane during dead-end filtration of tertiary wastewater, J. Membr. Sci., 191 (2001) 165–178.
[13] E. Barbot, P. Dussouillez, J.Y. Bottero, P. Moulin, Coagulation of bentonite suspension by polyelectrolytes or ferric chloride: Floc breakage and reformation, Chem. Eng. J., 156 (2010) 83–91.
[14] C. Henry, J.A. Brant, Mechanistic analysis of microfiltration membrane fouling by buckminsterfullerene (C60) nanoparticles, J. Membr. Sci., 415 (2012) 546–557.
[15] K.W. Trzaskus, W.M. de Vos, A. Kemperman, K. Nijmeijer, Towards controlled fouling and rejection in dead-end microfiltration of nanoparticles – Role of electrostatic interactions, J. Membr. Sci., 496 (2015) 174–184.
[16] K. Trzaskus, M. Elshof, A. Kemperman, K. Nijmeijer, Understanding the role of nanoparticle size and polydispersity in fouling development during dead-end microfiltration, J. Membr. Sci., 516 (2016) 152–161.
[17] K. W. Trzaskus, A. Zdeb, W. M. de Vos, A. Kemperman, K. Nijmeijer, Fouling behavior during microfiltration of silica nanoparticles and polymeric stabilizers, J. Membr. Sci., 505 (2016) 205–215.
[18] D. Jassby, S.-R. Chae, Z. Hendren, M. Wiesner, Membrane filtration of fullerene nanoparticle suspensions: Effects of derivatization, pressure, electrolyte species and concentration, J. Colloid Interface Sci., 346 (201) 296–302.
[19] N. Wu, Y. Wyart, L. Siozade, G. Georges, P. Moulin, Characterization of ultrafiltration membranes fouled by quantum dots by confocal laser scanning microscopy, J. Membr. Sci., 470 (2014) 40–51.
[20] J. Hermia, Constant pressure blocking filtration laws - Application to power-law non-newtonian fluids, Trans IChemE, 60 (1982) 111–120.
[21] A. Charfi, Etude d'un procédé membranaire de traitement des eaux usées: effet des paramètres biotiques et abiotiques sur le colmatage de la membrane, Université de Carthage, 2014.
[22] V.V. Tarabara, I. Koyuncu, M.R. Wiesner, Effect of hydrodynamics and solution ionic strength on permeate flux in cross-flow filtration: direct experimental observation of filter cake cross-sections, J. Membr. Sci., 241 (2004) 65–78.